J Solid State Electrochem (2012) 16:1595–1604
DOI 10.1007/s10008-011-1565-7

ORIGINAL PAPER

Growth and field crystallization of anodic films on Ta–Nb alloys

S. Komiyama · E. Tsuji · Y. Aoki · H. Habazaki · M. Santamaria · F. Di Quarto · P. Skeldon · G. E. Thompson

Received: 3 August 2011 / Revised: 28 September 2011 / Accepted: 30 September 2011 / Published online: 14 October 2011

Abstract The growth behavior of amorphous anodic films on Ta–Nb solid solution alloys has been investigated over a wide composition range at a constant current density of 50 $A\,m^{-2}$ in 0.1 mol dm^{-3} ammonium pentaborate electrolyte. The anodic films consist of two layers, comprising a thin outer Nb_2O_5 layer and an inner layer consisting of units of Ta_2O_5 and Nb_2O_5. The outer Nb_2O_5 layer is formed as a consequence of the faster outward migration of Nb^{5+} ions, compared with Ta^{5+} ions, during film growth under the high electric field. Their relative migration rates are independent of the alloy composition. The formation ratio, density, and capacitance of the films show a linear relation to the alloy composition. The susceptibility of the anodic films to field crystallization during anodizing at constant voltage increases with increasing niobium content of the alloy.

Keywords Anodic oxide · Nb–Ta alloys · Ionic transport · TEM · GDOES · RBS

S. Komiyama · E. Tsuji · Y. Aoki · H. Habazaki (✉)
Division of Materials Chemistry, Faculty of Engineering,
Hokkaido University,
Sapporo, Hokkaido 060-8628, Japan
e-mail: habazaki@eng.hokudai.ac.jp

M. Santamaria · F. Di Quarto
Dipartimento di Ingegneria Chimica dei Processi e dei Materiali,
Università degli Studi di Palermo,
Viale delle Scienze,
90128 Palermo, Italy

P. Skeldon · G. E. Thompson
Corrosion and Protection Centre, School of Materials,
The University of Manchester,
Manchester M13 9PL, UK

Introduction

Anodizing of valve metals under appropriate conditions enables the formation of barrier-type, usually amorphous, oxides of uniform thickness at high current efficiency. The anodic films have been extensively studied because of interest in ionic transport during the growth of anodic oxides under a high electric field [1–10] and for the important practical applications of anodic films, particularly in the capacitor industry [2, 11–19]. The anodic films are usually contaminated with species derived from electrolyte anions, and their depth distribution is controlled by the transport number of cations and anions during film growth and the mobility of incorporated electrolyte-derived species [20, 21]. The concentration of the electrolyte-derived species is usually less than 5 at.%, such that the control of film structure and properties by incorporation of electrolyte-derived species is limited.

The composition and properties of the anodic films can be controlled widely by using solid solution binary alloys as the substrate for anodizing. The change in band gap energy of "mixed oxide" with composition is also of fundamental interest [22]. Anodizing of tantalum alloys has been investigated for improving the dielectric properties of anodic Ta_2O_5, which is extensively used as a dielectric in the capacitor industry, as well as for increased understanding of the growth mechanism of anodic oxides [23–31]. Anodic Nb_2O_5 formed on niobium is also a promising dielectric for capacitor applications due to the high dielectric constant (ε_{ox}=42) compared with anodic Ta_2O_5 (ε_{ox}=27) [32, 33]. The higher permittivity of Nb_2O_5 suggests the possibility of achieving an increased capacitance of anodic Ta_2O_5 by incorporation of units of Nb_2O_5.

Here, we have examined the formation of anodic films on Ta–Nb alloys of various compositions in ammonium

pentaborate electrolyte. The compositional dependence of the growth behavior and film properties is examined. It is known that both anodic Nb_2O_5 and Ta_2O_5 undergo field crystallization during anodizing, particularly at higher formation voltages and at higher electrolyte temperatures [11, 12, 34, 35]. Since the field crystallization, which introduces regions of imperfection with a petal-like morphology, is detrimental for capacitor applications [36], the compositional dependence of the susceptibility to field crystallization of anodic films on the Ta–Nb alloys is also examined.

Experimental

Ta–Nb alloys containing 12, 22, 43, 70, and 87 at.% niobium, as well as tantalum and niobium metals, were deposited by DC magnetron sputtering using a Vacuum Products, SP-2C system. Targets of 99.9% pure tantalum of 100 mm in diameter, on which selected numbers of 99.9% niobium disks of 20-mm diameter were placed symmetrically and vice versa, were used for tantalum- and niobium-rich alloys, respectively. The sputtering chamber was evacuated to $\sim 5\times10^{-5}$ Pa and then sputtering was conducted in 99.999% argon (~0.3 Pa) at 0.5 A for 600 s. The substrates used for deposition of the layers were either glass plates or aluminum foils that had been electropolished and subsequently anodized to 200 V in 0.01 mol dm^{-3} ammonium pentaborate. The latter substrates were used for transmission electron microscopy observations and Rutherford backscattering spectroscopy (RBS) analysis. During deposition, the substrate holders were rotated around a central axis of chamber as well as their own axis to generate alloy films of uniform thickness and composition.

The deposited films were anodized to 80 V at a constant current density of 50 $A m^{-2}$ in stirred 0.1 mol dm^{-3} ammonium pentaborate aqueous electrolyte at 293 K using a Keithley 2400 source meter. A two-electrode cell with a platinum counter-electrode was used. The capacitance of the anodic films was examined by AC impedance spectroscopy at 1.5 V vs Ag/AgCl with AC amplitude of 50 mV (rms) over the frequency range of 1 Hz to 10 kHz in the same electrolyte using a NF Corporation 5020 frequency response analyzer and a Hokuto Denko HA501 potentiostat. For examination of field crystallization, the deposited films were anodized at 100 V in 0.1 mol dm^{-3} ammonium pentaborate aqueous electrolyte at 333 K for 3.6 ks. Prior to anodizing, some of the deposited specimens were thermally annealed at 523 K for 3.6 ks in air to accelerate the field crystallization.

The structures of the deposited alloy films were identified by X-ray diffraction (XRD) using a Rigaku RINT-2000 system with Cu Kα radiation. Ultramicrotomed sections, nominally ~10 nm in thickness, of the anodized specimens were examined in a JEOL JEM-2000FX transmission electron microscope operated at 200 kV. The surfaces of the anodized specimens were observed using a JEOL JSM-6500F field emission scanning electron microscope (SEM). Compositions of the alloy and anodic films were investigated by RBS, using 2.0 MeV He^{2+} ions supplied by a tandem-type accelerator at Institute for Materials Research, Tohoku University, with detection of scattered ions at 170°. Data were analyzed using the RUMP program. Further, depth profile analysis was conducted by glow discharge optical emission spectroscopy (GDOES) using a Jobin-Ybon 5000 instrument in an argon atmosphere of 600 Pa by applying RF of 13.56 MHz and power of 35 W. Light emissions of characteristic wavelengths were monitored throughout the analysis with a sampling time of 0.01 s to obtain elemental depth profiles. The wavelengths of the spectral lines used were 302.017, 416.466, 249.678, and 130.217 nm for tantalum, niobium, boron, and oxygen, respectively. The signals were detected from a circular area of approximately 4 mm in diameter. The XPS measurements of the thermally annealed specimens were carried out with a JEOL JPS-9200 spectrometer with a hemispherical energy analyzer and Mg Kα excitation (1,253.6 eV). The pressure in the analysis chamber during the XPS measurements was 1.0×10^{-7} Pa. The spectra were recorded at a 90° take-off angle with 0.1 eV step and 10 eV pass energy. The binding energy was calibrated by using the C 1s peak at 285.0 eV as the reference.

Results

Phases of the magnetron-sputtered Ta–Nb alloys

Figure 1 shows the XRD patterns of the magnetron-sputtered Ta–Nb alloys with a range of compositions. Tantalum and Ta–Nb alloys containing up to 22 at.% niobium comprised the β-Ta phase, with a tetragonal structure. The high-temperature β-Ta phase is often formed in physical vapor deposition of tantalum films. Further increase in the niobium content resulted in the formation of a bcc phase. A slight shift in the peaks of each phase occurred with change of the alloy composition. Since no peaks of second phase are evident, the alloys appear to be mainly single-phase solid solutions.

Characterization of anodic films

The deposited films were anodized at a constant current density of 50 $A m^{-2}$ to 80 V in 0.1 mol dm^{-3} ammonium pentaborate electrolyte at 293 K. The cell voltage increased

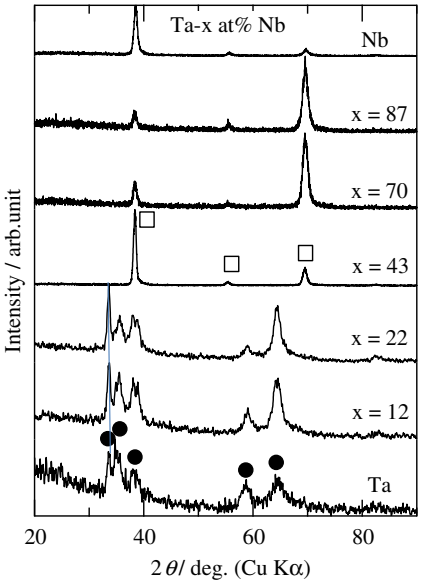

Fig. 1 XRD patterns of the magnetron-sputtered Ta–Nb alloy films of various compositions. *Unfilled square* denotes bcc phase and *filled circle* is β-Ta phase

linearly with anodizing time, with the slope depending upon the alloy composition. The slope changes linearly with alloy composition from 1.92 Vs^{-1} for tantalum to 1.41 Vs^{-1} for niobium (Fig. 2a). Transmission electron micrographs of ultramicrotomed sections of the specimens anodized to 80 V (Fig. 3) reveal thickening of the anodic films with increase in the niobium content in the alloy, consistent with the longer time required for anodizing the alloys with higher niobium contents. All the anodic films

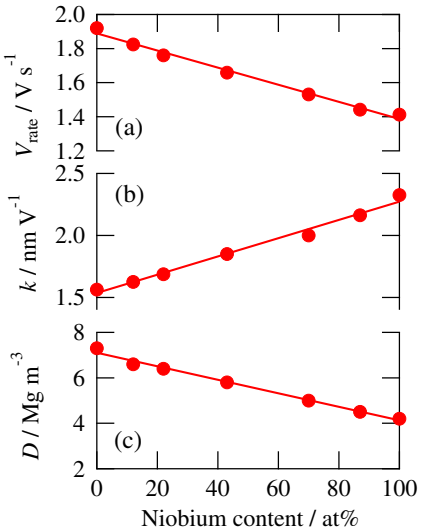

Fig. 2 Compositional dependence of **a** the rate of voltage rise, V_{rate}, during anodizing, **b** the formation ratio, k, and **c** the density, D, of the anodic films formed on the magnetron-sputtered Ta–Nb alloy films to 80 V at 50 Am^{-2} in 0.1 mol dm^{-3} ammonium pentaborate electrolyte at 293 K

are amorphous, regardless of alloy composition, as can be seen from their relatively featureless appearances; an example of a selected area diffraction pattern with diffuse halo rings is shown for the anodic film grown on the Ta–43 at.% Nb alloy (Fig. 3c). The formation ratios, k, of the anodic films, determined from the film thicknesses and the formation voltage, also change linearly with alloy composition from 1.56 nm V^{-1} for tantalum to 2.33 nm V^{-1} for niobium (Fig. 2b). The values for tantalum and niobium are in agreement with the reported ones [9].

The anodic films formed on the Ta–Nb alloys have a two-layered nature, although this is not obvious in the transmission electron micrographs. The presence of a thin outer Nb_2O_5 base layer, free from tantalum species, above a layer containing units of Ta_2O_5 and Nb_2O_5 is disclosed in GDOES depth profiles (Fig. 4). The outer layer appears to thicken with the niobium content in alloy. The total sputtering time of the anodic films also increases with the niobium content, and that for the Ta–87 at.% Nb alloy (Fig. 4e) is approximately twice that for the Ta–12 at.% Nb alloy (Fig. 4a). Since the thickness of the former anodic film is only 1.33 times that of the latter, the sputtering rate of the anodic films may be reduced with an increase in the niobium content. It is clear from Fig. 4 that boron species from the electrolyte are incorporated into the outer part of the films. The distribution of the boron species, estimated from the sputtering time, is not dependent upon the film composition, the boron being located in the outer ~0.2 of the film thicknesses. These depths are similar to that on niobium (0.15) [37]. The peak intensity of boron relative to the oxygen intensity in the anodic films decreases with increase in the niobium content in alloy, suggesting that the amount of boron species in the anodic films decreases with the niobium content. Due to the absence of suitable boron standard materials for quantification, the actual boron concentrations in the anodic films have not been analyzed.

Apart from boron species, the compositions of the anodic films have been examined quantitatively using RBS. In the RBS analysis, boron species were neglected due to low sensitivity for boron. Examples of experimental and simulated RBS spectra for the as-deposited and anodized Ta–43 at.% Nb specimens are shown in Fig. 5. Figure 5b reveals the shift of the leading edge for tantalum to a lower energy after anodizing, in agreement with the presence of an outer tantalum-free Nb_2O_5 layer. As in Fig. 5, the simulated spectra for all the specimens fitted well with the respective experimental ones, and the compositions, thicknesses, and densities of anodic films, obtained by RBS, are summarized in Table 1. Two-layered anodic films form on all the alloys, with the relative thickness of the outer Nb_2O_5 layer decreasing with reducing niobium content in alloy. Even on the Ta–87 at.% Nb alloy, the thickness of the outer layer relative to the

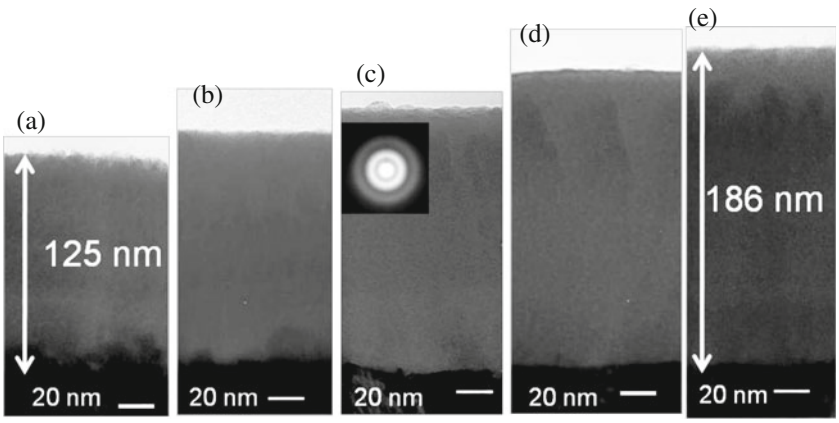

Fig. 3 Transmission electron micrographs of ultramicrotomed sections of the anodic oxide films formed on the magnetron-sputtered **a** Ta, **b** Ta–12 at.% Nb, **c** Ta–43 at.% Nb, **d** Ta–87 at.% Nb, and **e** Nb films to 80 V at 50 Am^{-2} in 0.1 mol dm^{-3} ammonium pentaborate electrolyte at 293 K

total film thickness is less than 0.07. The inner layer contains both units of Ta_2O_5 and Nb_2O_5, and the ratio of tantalum to niobium in the inner layer is slightly higher than that in the respective alloy substrate due to the ejection of Nb_2O_5 to form the outer layer. The growth of anodic oxides at high current efficiency was also confirmed from the fact that the charge passed during anodizing was close to that calculated from the amounts of pentavalent niobium and tantalum ions in the anodic films. The linear change in density, *D*, of the inner layer of anodic oxides with alloy composition (composition of inner layer) is displayed in Fig. 2c.

Dielectric properties

The dielectric properties of anodic films have been examined by AC impedance. Figure 6 shows the Bode diagrams of the tantalum, Ta–43 at.% Nb, and niobium specimens anodized to 80 V. All the specimens show a linear impedance change with frequency over a wide frequency range with a slope close to 90° and phase shift of nearly −90° in the intermediate frequency range, which are typical of dielectric materials. The other alloy specimens anodized to 80 V also revealed similar impedance spectra.

Using the equivalent circuit shown in Fig. 6, the capacitances of the anodic films were determined. Although a thin outer layer of Nb_2O_5 is present on all the alloys, the two-layered structure of the films could not be identified by the impedance spectra due to similar time constants for the outer and inner layers. Thus, the single-layer model was used to fit the impedance spectra. The compositional dependence of the capacitance of the anodic films, together with the film thickness and permittivity, is plotted in Fig. 7.

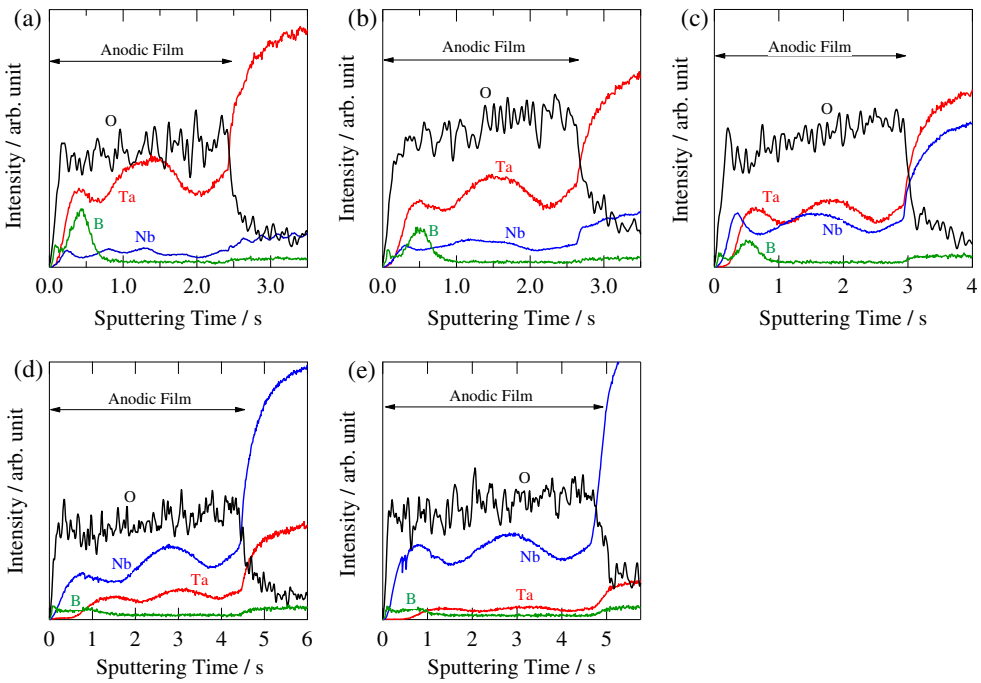

Fig. 4 GDOES elemental depth profiles of the anodic oxide films formed on the magnetron-sputtered **a** Ta–12 at.% Nb, **b** Ta–22 at.% Nb, **c** Ta–43 at.% Nb, **d** Ta–70 at.% Nb, and **e** Ta–87 at.% Nb films to 80 V at 50 Am^{-2} in 0.1 mol dm^{-3} ammonium pentaborate electrolyte at 293 K

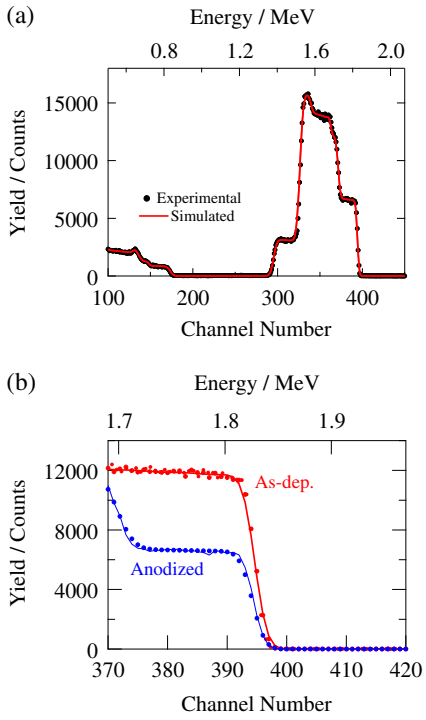

Fig. 5 **a** Experimental and simulated RBS spectra of the magnetron-sputtered Ta–43 at.% Nb alloy film anodized to 80 V at 50 Am^{-2} in 0.1 mol dm^{-3} ammonium pentaborate electrolyte at 293 K. **b** Tantalum yield region of experimental and simulated RBS spectra of the magnetron-sputtered Ta–43 at.% Nb alloy film as deposited and anodized to 80 V at 50 Am^{-2} in 0.1 mol dm^{-3} ammonium pentaborate electrolyte at 293 K

In all cases, a linear correlation is revealed. The following relation holds between the capacitance, C_p, film thickness, d, and permittivity, ε_{ox}:

$$C_p = \varepsilon_0 \varepsilon_{ox} S/d$$

in which ε_0 is the permittivity of vacuum and S is the surface area. The increase in C_p with niobium content indicates that the increase in ε_{ox} is larger than the thickening of the anodic oxide by the addition of niobium.

Field crystallization

As shown in Fig. 3, the anodic films formed on Ta–Nb alloys as well as tantalum and niobium are amorphous, but field crystallization of amorphous anodic oxides has been reported for anodic Ta_2O_5 and Nb_2O_5 at high voltages in electrolytes at elevated temperatures [11, 12, 34–36, 38–43]. The field crystallization is detrimental for capacitor applications due to degradation of the electric properties: increased leakage current and dielectric dissipation factor [44]. Here, the compositional dependence of the behavior of field crystallization of anodic oxides on the Ta–Nb alloys has been investigated at 100 V in 0.1 mol dm^{-3} ammonium pentaborate electrolyte at 333 K. Figure 8a shows the current transients during anodizing of the Ta–Nb alloys as well as tantalum and niobium at 100 V for 3.6 ks. Figure 9 shows the SEM surface images of the resultant anodic films. The current transients (Fig. 8a) reveal a linear current decrease with time in a double logarithmic plot, as expected from the high-field film growth kinetics [45]. However, the current increases for niobium after anodizing for ~1 ks. The change in behavior is associated with field crystallization, and crystallized circular regions are evident in Fig. 9e. The Ta–87 at.% Nb alloy also shows a slight deviation from the linear current decrease, and Fig. 9d shows the presence of crystalline regions. The size of the regions on the Ta–87 at.% Nb alloy is smaller than that on niobium, and their population density is also reduced on the alloy. Thus, the deviation in the current transient is much smaller for the Ta–87 at.% Nb alloy than for niobium. The other alloys and tantalum showed a continuous linear decay of current, but crystalline regions are also present on the Ta–70 at.% Nb alloy, although the regions are of much smaller size and of lower population density. No field crystallization was found for anodizing under the present conditions when the tantalum content is further increased. The findings indicate that the susceptibility to field crystallization increases with increase in the niobium content in alloy.

Table 1 Results of RBS analyses for anodic oxide films formed on the magnetron-sputtered Ta–Nb alloys to 80 V at 50 Am^{-2} in 0.1 mol dm^{-3} ammonium pentaborate electrolyte at 293 K

Alloy composition	Anodic oxide film		
	Thickness (nm), outer layer/inner layer	Composition, outer layer/Inner layer	Density (Mg m^{-3}), outer layer/inner layer
Ta	125	Ta_2O_5	7.3
Ta–12 at.% Nb	2.5/128	$Nb_2O_5/(Ta_{0.89}Nb_{0.11})_2O_5$	4.2/6.6
Ta–22 at.% Nb	3/132	$Nb_2O_5/(Ta_{0.80}Nb_{0.20})_2O_5$	4.2/6.4
Ta–43 at.% Nb	4/144	$Nb_2O_5/(Ta_{0.59}Nb_{0.41})_2O_5$	4.2/5.8
Ta–70 at.% Nb	8/155	$Nb_2O_5/(Ta_{0.31}Nb_{0.69})_2O_5$	4.2/5.0
Ta–87 at.% Nb	12/168	$Nb_2O_5/(Ta_{0.14}Nb_{0.86})_2O_5$	4.2/4.5
Nb	186	Nb_2O_5	4.2

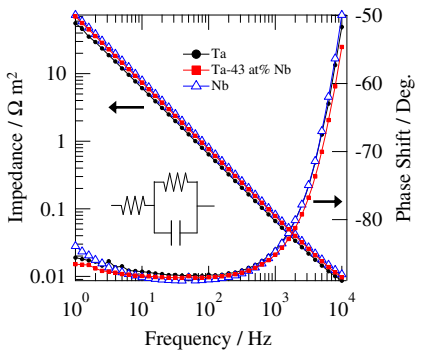

Fig. 6 Bode diagrams of the magnetron sputtered Ta, Ta–43 at.% Nb, and Nb films anodized to 80 V at 50 Am^{-2} in 0.1 mol dm^{-3} ammonium pentaborate electrolyte at 293 K

It is known that the air-formed oxide or thermal oxide that is present on the surface before anodizing becomes an initiation site of field crystallization of anodic Nb_2O_5. Thus, prior thermal treatment enhances the field crystallization [41]. Figure 8b shows the current transients of the specimens with prior thermal treatment at 523 K during anodizing at 100 V. As in the previous study, the deviation from the linear current decrease is more marked for the niobium specimen thermally treated at 523 K, and a higher population density of crystalline regions is found on the surface of the anodic film by SEM observation (Fig. 10e). However, no significant influence of prior thermal treatment on the current transient is observed for the Ta–Nb alloys as well as tantalum. In fact, the surfaces of the tantalum and Ta–43 at.% Nb specimens subjected to prior thermal treatment are smooth after anodizing and no obvious evidence of crystallization is found (Fig. 10a, b).

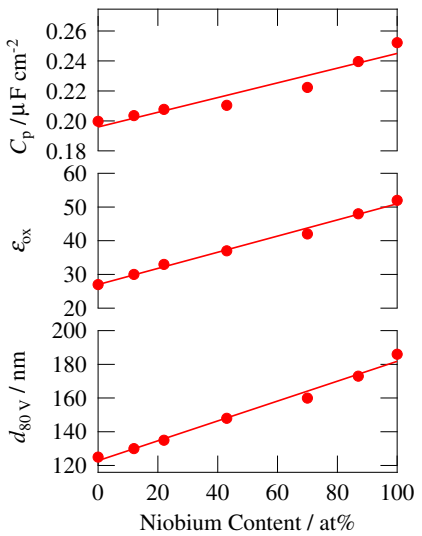

Fig. 7 Compositional dependence of **a** the capacitance, C_p, **b** the permittivity, ε_{ox}, and **c** the thickness, d_{80V}, of the anodic oxide films formed on the magnetron-sputtered Ta–Nb alloy films to 80 V at 50 Am^{-2} in 0.1 mol dm^{-3} ammonium pentaborate electrolyte at 293 K

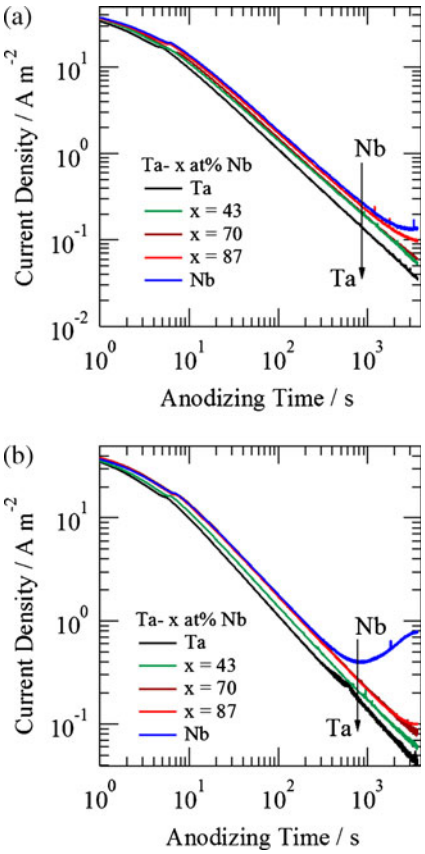

Fig. 8 Current transient during anodizing of the **a** as-deposited and **b** thermally treated Ta, Ta–Nb alloys, and Nb films at 100 V in 0.1 mol dm^{-3} ammonium pentaborate electrolyte at 333 K. The thermal treatment was carried out in air at 523 K for 3.6 ks

Clear acceleration of field crystallization by the prior thermal treatment is revealed only for niobium. However, a slight acceleration may occur for the Ta–87 at.% Nb alloy since the population density of the crystalline regions appears to be increased by the prior thermal treatment.

Discussion

In the present study, the compositional dependence of the properties of anodic films, such as formation ratio, density, and permittivity, has been examined on the Ta–Nb single-phase alloys. These parameters change linearly with alloy composition between the values of anodic Ta_2O_5 and Nb_2O_5. The finding is characteristic for amorphous anodic oxides on binary alloys. A similar compositional dependence was reported for amorphous oxide films on Al–Ta [46–48] and Al–Hf [49] alloys. The compositional dependence of the properties of "mixed" amorphous oxides contrasts with that of crystalline anodic oxides formed on binary alloys. Typical examples that show a marked enhancement of the capacitance at particular compositions for Zr–Si and Zr–Al alloys have been reported recently [50,

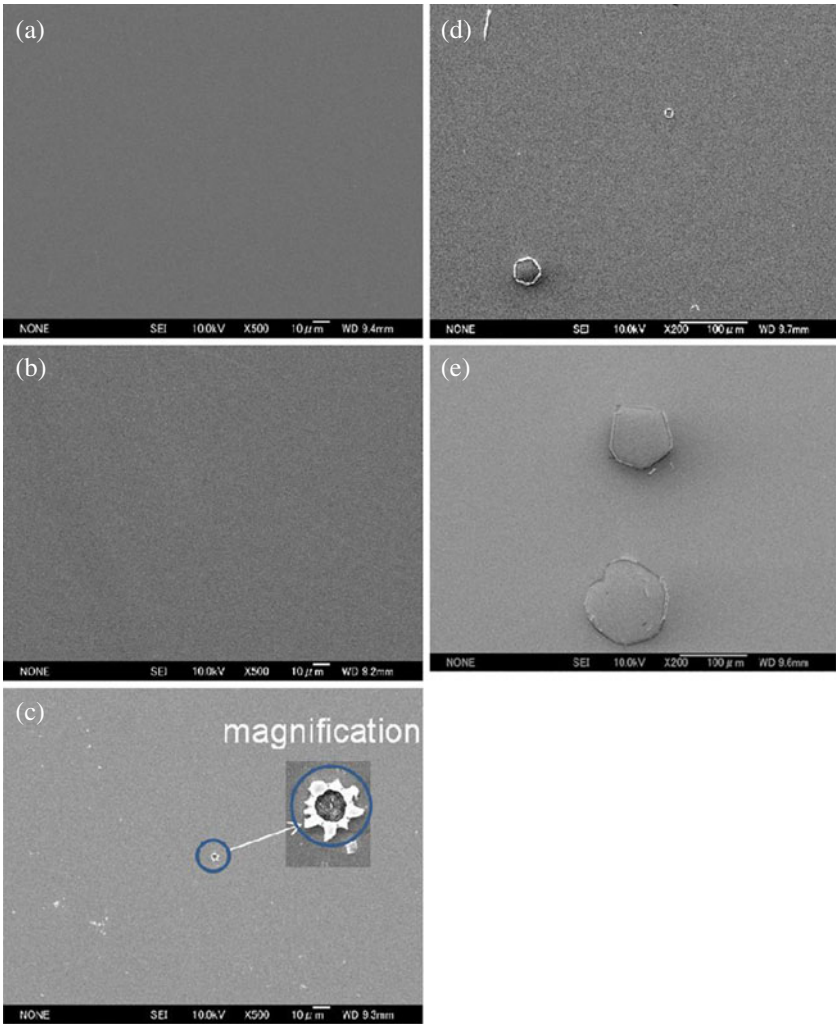

Fig. 9 Scanning electron micrographs of the surfaces of the magnetron-sputtered **a** Ta, **b** Ta–43 at.% Nb, **c** Ta–70 at.% Nb, and **d** Ta–87 at.% Nb and **e** Nb films anodized at 100 V in 0.1 mol dm^{-3} ammonium pentaborate electrolyte at 333 K for 3.6 ks

51]. The precipitation of nanocrystalline tetragonal ZrO_2 phase with high permittivity enhances the permittivity of the anodic oxide and the resultant enrichment of silicon or aluminum species in the surrounding amorphous matrix reduces the film thickness.

A two-layered anodic film is formed on the Ta–Nb alloys, comprising a thin outer Nb_2O_5 layer and an inner layer containing both units of Ta_2O_5 and Nb_2O_5. Amorphous anodic oxides, including Ta_2O_5 and Nb_2O_5, grow both at the metal/film and film electrolyte interfaces by a cooperative transport of O^{2-} ions inward and cations outward, respectively. The transport number of cations is similar for anodic Ta_2O_5 and Nb_2O_5 [9]; under the present anodizing conditions, the transport number of cations is 0.3 for anodic Nb_2O_5 [52], and a similar value is expected from the change in the transport number of cations with current density for anodic Ta_2O_5 [53]. In this case, in the present anodic films on the Ta–Nb alloys, both Nb^{5+} and Ta^{5+} ions migrate outward, with the greater rate for the former cations. The slower migration of Ta^{5+} ions with respect to Nb^{5+} ions is correlated with the stronger Ta^{5+}–O bond (347 kJ mol^{-1}) compared with the Nb^{5+}–O bond (329 kJ mol^{-1}). The good correlation between the relative migration rates of the two cations and their metal–oxygen bond strengths has been found for many amorphous anodic oxides formed on binary alloys, including Al–Ta, Al–Zr, Al–Hf, Al–Sm, Al–Mo, Al–W, Ti–W, Ti–Mo, Ti–Si, and Nb–Si alloys [47, 49, 52, 54–63]. The correlation suggests the importance of breakage of the metal–oxygen bonds in the ionic transport in growing amorphous anodic oxides under the high electric field. As a consequence of the bond breakage, counter-migration of cations and anions occurs. Several models of ionic migration have been proposed, ranging from early suggestions of vacancy diffusion and interstitial exchange capture [3] and a place exchange mechanism [8] to a liquid droplet mechanism [10]. A more recent defect cluster mechanism correlates the transport number of cations and field strength [64].

The relative migration rate of Ta^{5+} ions, with respect to Nb^{5+} ions, is calculated from the number of Nb^{5+} ions in

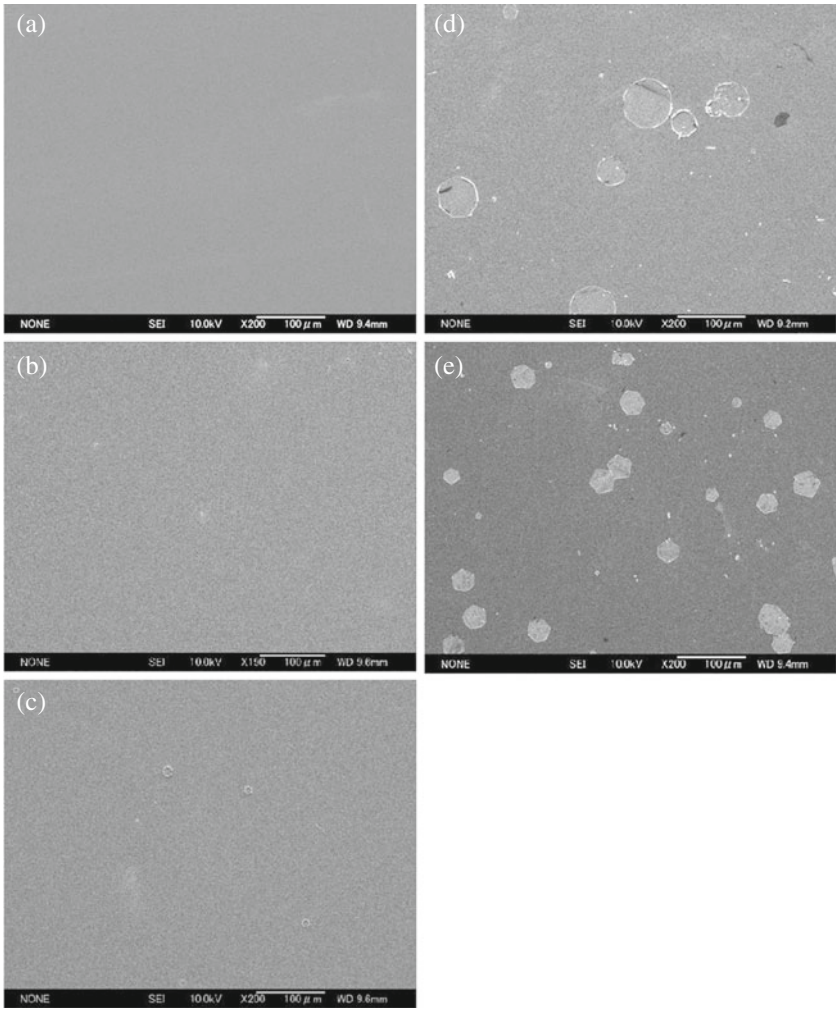

Fig. 10 Scanning electron micrographs of the surfaces of the magnetron-sputtered **a** Ta, **b** Ta–43 at.% Nb, **c** Ta–70 at.% Nb, and **d** Ta–87 at.% Nb and **e** Nb films thermally treated in air at 523 K for 3.6 ks and subsequently anodized at 100 V in 0.1 mol dm^{-3} ammonium pentaborate electrolyte at 333 K for 3.6 ks

the region of inner layer above the marker plane to the total number of Nb^{5+} ions in the entire film region above the marker plane, which is assumed to be with depth of 0.3 of the total film thickness. The calculation revealed that the migration rate of Ta^{5+} ions was ~0.75 that of Nb^{5+} ions, regardless of alloy composition. The Ta^{5+} ions also migrate slower than Al^{3+} ions in the anodic films on Al–Ta alloys, with the relative Ta^{5+} migration rate increasing with tantalum content [47, 48]. The enhanced relative migration rate of Ta^{5+} ions was explained by the increased Lorentz field. The Lorentz field in anodic Ta_2O_5 is approximately twice that of anodic Al_2O_3, while the field of anodic Nb_2O_5 is only ~1.2 times that of anodic Ta_2O_5. The composition-independent relative migration rate of Ta^{5+} ions in the present anodic films may be due to the relatively small change in the Lorentz field with film composition.

No field crystallization of the anodic oxide occurred on tantalum at 100 V in 0.1 mol dm^{-3} ammonium pentabrate electrolyte at 333 K, whereas crystalline oxide is formed on niobium under the same anodizing conditions. The niobium-rich Ta–Nb alloys also suffered field crystallization. The finding indicates a higher susceptibility of field crystallization of anodic Nb_2O_5 compared with anodic Ta_2O_5. For complete suppression of field crystallization under the present condition, more than 30 at.% tantalum must be added to niobium, while for silicon addition as an alloying element to niobium, 12 at.% is sufficient [43]. Field crystallization is also known for anodic TiO_2 [65–67]. Alloying of titanium also impedes the crystallization, and it has been found that the more slowly migrating or immobile alloying element species suppress more effectively the field crystallization of anodic TiO_2 [68]. Ta^{5+} ions migrate outward at a slightly slower rate than Nb^{5+} ions, as discussed above, while silicon species are immobile. Thus, it is likely that also for field crystallization of anodic Nb_2O_5, incorporation of more slowly migrating or immobile species impedes the crystallization more effectively.

Prior thermal treatment of niobium accelerates the field crystallization of anodic Nb_2O_5 [41], as also confirmed in the present study. Compared with anodic Nb_2O_5, the acceleration is limited for anodic oxides on niobium-rich

Ta–Nb alloys, and no crystallization is evident for the tantalum-rich alloys. The oxide formed by the prior thermal treatment becomes a nucleation site of crystalline oxide so that field crystallization is accelerated. The presence of both units of Ta_2O_5 and Nb_2O_5 in the thermal oxide films on the Ta–Nb alloys was confirmed by X-ray photoelectron spectroscopy and the "mixed oxides" might be more resistive for nucleation of crystalline oxides compared with thermally formed Nb_2O_5.

Conclusions

1. Anodizing of magnetron-sputtered Ta–Nb alloys of a range of compositions in ammonium pentaborate electrolyte at high current efficiency results in the formation of two-layered amorphous anodic films, comprising a thin outer relatively pure Nb_2O_5 layer and an inner layer consisting of both units of Ta_2O_5 and Nb_2O_5.
2. The films grow by migration of cations and anions, with slower migration of Ta^{5+} ions relative to Nb^{5+} ions, leading to two-layered films. The migration rate of Ta^{5+} ions is ~0.75 that of Nb^{5+} ions, regardless of the alloy composition, and the slower migration of Ta^{5+} ions correlates with the stronger Ta^{5+}–O bond relative to the Nb^{5+}–O bond. Boron species, incorporated from electrolyte, are present in the outer ~20% of the film thickness; such species also migrate outward.
3. The film properties, i.e., formation ratio, density, and permittivity, change approximately linearly with alloy composition.
4. Susceptibility to field crystallization of the anodic film increases with increase of niobium content of the alloy.

References

1. Vermilyea DA (1960) Kinetics of ion motion in anodic oxide films. Non-Cryst Solids, Conf Alfred, New York: 328–347
2. Young L (1961) Anodic oxide films. Academic, London
3. Amsel G, Samuel D (1962) The mechanism of anodic oxidation. J Phys Chem Solids 23:1707–1718
4. Davies JA, Domeij B, Pringle JPS, Brown F (1965) The migration of metal and oxygen during anodic film formation. J Electrochem Soc 112:675–680
5. Dignam MJ (1972) Ionic transport through oxide films. In: Diggle JW (ed) Oxide and oxide films, vol 1. Marcel Dekker, New YorK, pp 91–286
6. Cherki C, Siejka J (1973) Study by nuclear microanalysis and O^{18} tracer techniques of the oxygen transport processes and the growth laws for porous anodic oxide layers on aluminum. J Electrochem Soc 120:784–791
7. Mackintosh WD, Brown F, Plattner HH (1974) Mobility of metallic foreign atoms during the anodic oxidation of aluminum. J Electrochem Soc 121:1281–1286
8. Fromhold AT (1980) Nonsimultaneous place exchange: a microscopic high field transport mechanism in solids. J Electrochem Soc 127:411–425
9. Pringle JPS (1980) The anodic oxidation of superimposed metallic layers: theory. Electrochim Acta 25:1423–1437
10. Mott NF (1987) On the oxidation of silicon. Philos Mag B 55:117–129
11. Vermilyea DA (1955) The crystallization of anodic tantalum oxide films in the presence of a strong electric field. J Electrochem Soc 102:207–214
12. Lakhiani DM, Shreir LL (1960) Crystallization of amorphous Nb oxide during anodic oxidation. Nature 188:49–50
13. Alwitt RS (1981) Crystalline anodic oxide films on aluminium. J Met Surf Finish Soc Jpn 32:226–229
14. Boiko BT, Kopach VR, Panchekha PA, Pozdeev YL (1988) Composition and electrical properties of oxide films on nitrided niobium. Izv Vyssh Uchebn Zaved Fiz 31(10):115–116
15. Boiko BT, Panchekha PA, Kopach VR, Pozdeev YL, Bagatskaya EV, Melent'ev SB (1988) Structural processes in a niobium layer in contact with niobium pentoxide. Fiz Khim Obrab Mater 5:61–67
16. Boiko BT, Konach VR, Panchekha PA, Pozdeev YL, Starikov VV (1991) Modeling degradation processes in tantalum and niobium oxide—semiconductor capacitors. Elektron Tekhn Ser 8(1):27–30
17. Boiko BT, Kopach VR, Krushedol'skaya NG, Panchekha PA, Pozdeev YL, Starikov VV (1991) Influence of vacuum annealing on the asymmetry of tantalum pentoxide film conductivity. Izv Vyssh Uchebn Zaved Fiz 34(1):46–50
18. Pozdeev Y (1998) Reliability comparison of tantalum and niobium solid electrolytic capacitors. Qualt Reliab Eng Int 14:79–82
19. Tauseef Tanvir M, Aoki Y, Habazaki H (2009) Formation of porous niobium films by oblique angle deposition: influence of substrate morphology. Thin Solid Films 517(24):6711–6716
20. Shimizu K, Kobayashi K, Thompson GE, Skeldon P, Wood GC (1996) Anodic oxide films on tantalum: incorporation and mobilities of electrolyte-derived species. Philos Mag B 73 (3):461–485
21. Wood GC, Skeldon P, Thompson GE, Shimizu K (1996) A model for the incorporation of electrolyte species into anodic alumina. J Electrochem Soc 143:74–83
22. Santamaria M, Di Quarto F, Habazaki H (2008) Photocurrent spectroscopy applied to the characterization of passive films on sputter-deposited Ti–Zr alloys. Corros Sci 50(7):2012–2020
23. Silverman PJ, Schwartz N (1974) A Rutherford scattering analysis of anodic tantalum–silicon oxides. J Electrochem Soc 121:550–555
24. Ruth RL, Schwartz N (1976) A Rutherford backscattering analysis of anodic tantalum–titanium oxides. J Electrochem Soc 123:1860–1867
25. Labunov V, Sokol V, Vorobiova A, Bondarenko V (1985) AES analysis of anodic tantalum–aluminium oxide films. Electrochim Acta 30(8):1079–1084
26. Werder DJ, Kola RR (1998) Microstructure of Ta_2O_5 films grown by the anodization of TaN_x. Thin Solid Films 323:6–9
27. Duenas S, Castan E, Barbolla J, Kola RR, Sullivan PA (2001) Tantalum pentoxide obtained from TaN_x and $TaSi_2$ anodisation: an inexpensive and thermally stable high k dielectric. Solid State Electron 45:1441–1450
28. Mato S, Thompson GE, Skeldon P, Shimizu K, Habazaki H, Masheder D (2001) Enrichment of alloying elements beneath anodic oxides: investigation of Ta–1.5 at.% Cu alloy. Corros Sci 43(5):993–1002
29. Mato S, Alcala G, Skeldon P, Thompson GE, Mann AB, Masheder D, Habazaki H, Shimizu K (2003) Dielectric and

mechanical properties of anodic films in the Ta–Ti system. Surf Interface Anal 35(5):477–482
30. Mato S, Alcala G, Skeldon P, Thompson GE, Quance T, Graham MJ, Habazaki H, Shimizu K, Masheder D (2003) Oxygen generation in anodized Ta–Cu alloys. Philos Mag 83(23):2733–2746
31. Mato S, Alcala G, Thompson GE, Skeldon P, Shimizu K, Habazaki H, Quance T, Graham MJ, Masheder D (2003) Anodic oxidation of Ta/Fe alloys. Corros Sci 45(12):2881–2892
32. Kovacs K, Kiss G, Stenzel M, Zillgen H (2003) Anodic oxidation of niobium sheets and porous bodies heat-treatment of the Nb/Nb-oxide system. J Electrochem Soc 150(8):B361–B366
33. Stormer H, Weber A, Fischer V, Ivers-Tiffee E, Gerthsen D (2009) Anodically formed oxide films on niobium: microstructural and electrical properties. J Eur Ceram Soc 29(9):1743–1753
34. Jackson NF (1973) Field crystallization of anodic films on tantalum. J Appl Electrochem 3:91–94
35. Vermilyea DA (1957) Nucleation of crystalline tantalum pentoxide during field crystallization. J Electrochem Soc 104:542–546
36. Nagahara K, Sakairi M, Takahashi H, Matsumoto K, Takayama K, Oda Y (2004) Change in the structure and dielectric properties of niobium anodic oxide films during potentiostatic anodizing. Elechemistry 72(9):624–632
37. Habazaki H, Matsuo T, Konno H, Shimizu K, Nagata S, Takayama K, Oda Y, Skeldon P, Thompson GE (2003) Formation of N_2O gas bubbles in anodic films on NbN_x alloys. Thin Solid Films 429(1–2):159–166
38. Jackson NF, Hendy JC (1974) Use of niobium as an anode material in liquid filled electrolytic capacitors. Electrocompon Sci Technol 1:27–37
39. Asoh H, Odate H, Ono S (2004) Crystallization and dielectric properties of anodic oxide films formed on niobium. J Surf Finish Soc Jpn 55(12):952–959
40. Habazaki H, Ogasawara T, Konno H, Shimizu K, Asami K, Nagata S, Takayama K, Skeldon P, Thompson G Field crystallization of anodic niobia on Nb–O substrates In: Fujimoto S, Akiyama E, Habazaki H, Macdougall B (eds) ECS Trans, Los Angeles, 2006. vol 4. The Electrochemical Society, pp 343–349
41. Habazaki H, Ogasawara T, Konno H, Shimizu K, Nagata S, Skeldon P, Thompson GE (2007) Field crystallization of anodic niobia. Corros Sci 49(2):580–593
42. Nagahara K, Sakairi M, Takahashi H, Matsumoto K, Takayama K, Oda Y (2007) Mechanism of formation and growth of sunflower-shaped imperfections in anodic oxide films on niobium. Electrochim Acta 52(5):2134–2145
43. Habazaki H, Ogasawara T, Fushimi K, Shimizu K, Nagata S, Izumi T, Skeldon P, Thompson GE (2008) Inhibition of field crystallization of anodic niobium oxide by incorporation of silicon species. Electrochim Acta 53(28):8203–8210
44. Nagahara K, Sakairi M, Takahashi H, Nagata S, Matsumoto K, Takayama K, Oda Y (2004) Influence of current density on the structure and dielectric properties of anodic oxide films on niobium. J Surf Finish Soc Jpn 55(12):943–951
45. Cabrera N, Mott NF (1949) Theory of the oxidation of metals. Rep Prog Phys 12:163–184
46. Luby S (1976) Dielectric properties of anodic oxides formed on sputtered Ta–Al alloy films. Thin Solid Films 32(1):61–64
47. Habazaki H, Shimizu K, Skeldon P, Thompson GE, Wood GC (1997) Inter-relationships between ionic transport and composition in amorphous anodic oxides. Proc R Soc Lond A 453:1593–1609
48. Alcala G, Mato S, Skeldon P, Thompson GE, Bailey P, Noakes TCQ, Habazaki H, Shimizu K (2003) Anodic film growth in the Al–Ta alloy system. Corros Sci 45(8):1803–1813
49. Fogazza M, Santamaria M, Di Quarto F, Garcia-Vergara SJ, Molchan I, Skeldon P, Thompson GE, Habazaki H (2009) Formation of anodic films on sputtering-deposited Al–Hf alloys. Electrochim Acta 54(3):1070–1075
50. Koyama S, Aoki Y, Sakaguchi N, Nagata S, Habazaki H (2010) Phase transformation and capacitance enhancement of anodic ZrO_2–SiO_2. J Electrochem Soc 157(12):C444–C451
51. Koyama S, Aoki Y, Nagata S, Habazaki H (2011) Formation and dielectric properties of anodic oxide films on Zr–Al alloys. J Solid State Electrochem. doi:10.1007/s10008-010-1238-y
52. Habazaki H, Matsuo T, Konno H, Shimizu K, Nagata S, Matsumoto K, Takayama K, Oda Y, Skeldon P, Thompson GE (2003) Influence of silicon species on the electric properties of anodic niobia. Electrochim Acta 48(23):3519–3526
53. Lu Q, Skeldon P, Thompson GE, Masheder D, Habazaki H, Shimizu K (2004) Transport numbers of metal and oxygen species in anodic tantala. Corros Sci 46(11):2817–2824
54. Habazaki H, Skeldon P, Thompson GE, Wood GC, Shimizu K (1997) Anodic film formation on a sputter-deposited amorphous Al–40 at.% Sm alloy. J Mater Res 12(7):1885–1891
55. Habazaki H, Shimizu K, Skeldon P, Thompson GE, Wood GC (1996) The composition of the alloy/film interface during anodic oxidation of Al–W alloys. J Electrochem Soc 143:2465–2470
56. Habazaki H, Skeldon P, Thompson GE, Wood GC, Shimizu K (1995) Direct observation of an anodic film on a sputter-deposited amorphous Al–W alloy. Philos Mag B 71(1):81–90
57. Habazaki H, Skeldon P, Shimizu K, Thompson GE, Wood GC (1995) Anodic film formation on a sputter-deposited Al–30 at.% Mo alloy. Corros Sci 37(9):1497–1509
58. Habazaki H, Skeldon P, Shimizu K, Thompson GE, Wood GC (1995) Anodic film formation on sputter-deposited amorphous Al–Zr alloys. J Phys D Appl Phys 28(12):2612–2618
59. Habazaki H, Uozumi M, Konno H, Shimizu K, Nagata S, Takayama K, Oda Y, Skeldon P, Thompson GE (2005) Influence of film composition on the structure and dielectric properties of anodic films on Ti–W alloys. J Electrochem Soc 152(8):B263–B270
60. Habazaki H, Uozumi M, Konno H, Shimizu K, Nagata S, Asami K, Skeldon P, Thompson GE (2002) Influence of molybdenum species on growth of anodic titania. Electrochim Acta 47 (24):3837–3845
61. Habazaki H, Shimizu K, Nagata S, Skeldon P, Thompson GE, Wood GC (2002) Ionic mobilities in amorphous anodic titania. J Electrochem Soc 149:B70–B74
62. Habazaki H, Shimizu K, Nagata S, Skeldon P, Thompson GE, Wood GC (2002) Ionic transport in amorphous anodic titania stabilised by incorporation of silicon species. Corros Sci 44:1047–1055
63. Habazaki H, Fushimi K, Konno H, Shimizu K, Asami K, Skeldon P, Thompson GE (2006) Origin of hydrogen in anodized niobium. J Surf Finish Soc Jpn 57:676–678
64. Wang M-H, Hebert KR (1999) Metal and oxygen ion transport during ionic conduction in amorphous anodic oxide films. J Electrochem Soc 146(10):3741–3749
65. Habazaki H, Uozumi M, Konno H, Shimizu K, Skeldon P, Thompson GE (2003) Crystallization of anodic titania on titanium and its alloys. Corros Sci 45(9):2063–2073
66. Shibata T, Zhu Y-C (1995) The effect of film formation conditions on the structure and composition of anodic oxide films on titanium. Corros Sci 37:253–270
67. Dyer CK, Leach JSL (1978) Breakdown and efficiency of anodic oxide growth on titanium. J Electrochem Soc 125:1032–1038
68. Habazaki H, Konno H, Shimizu K (2003) Structure and growth behavior of anodic oxide films on titanium and its alloys. J Surf Finish Soc Jpn 54(7):456–461